

Geophysical Research Letters

RESEARCH LETTER

10.1029/2019GL086165

Key Points:

- The role of mesoscale ocean temperature anomalies in modifying tropical cyclone characteristics is discussed
- Size changes endure and destructive potential depends on the integrated history of ocean temperature exposure
- Gale force wind radius, integrated kinetic energy, and angular momentum fluxes correlate with storm total precipitation

Supporting Information:

- Supporting Information S1

Correspondence to:

N. Bruneau,
 bruneau.n@gmail.com

Citation:

Bruneau, N., Wang, S., & Toumi, R. (2020). Long memory impact of ocean mesoscale temperature anomalies on tropical cyclone size. *Geophysical Research Letters*, 47, e2019GL086165. <https://doi.org/10.1029/2019GL086165>

Received 14 NOV 2019

Accepted 2 MAR 2020

Accepted article online 4 MAR 2020

Corrected 12 APR 2020

This article was corrected on 12 APR 2020. See the end of the full text for details.

©2020. The Authors.

This is an open access article under the terms of the Creative Commons Attribution License, which permits use, distribution and reproduction in any medium, provided the original work is properly cited.

Long Memory Impact of Ocean Mesoscale Temperature Anomalies on Tropical Cyclone Size

N. Bruneau^{1,2} , S. Wang^{1,3} , and R. Toumi¹

¹Blackett Laboratory, Department of Physics, Imperial College, London, UK, ²National Oceanography Centre, Liverpool, UK, ³State Key Laboratory of Satellite Ocean Environment Dynamics, Second Institute of Oceanography, Ministry of Natural Resources, Hangzhou, China

Abstract Mesoscale ocean temperature anomalies modify a tropical cyclone (TC). Through a modeling study we show that, while the maximum wind speed is rapidly restored after the TC passes a warm- or cold- (eddy size) sea surface temperature (SST) anomaly, the storm size changes are more significant and persistent. The radius of gale force winds and integrated kinetic energy (IKE) can change by more than 10% per degree and this endures several days after crossing an SST anomaly. These properties have a long memory of the impact from the ocean fluxes and depend on the integrated history of SST exposure. They are found to be directly proportional to the storm total precipitation. Accurate continuous forecast of the SST along the track may therefore be of central importance to improving predictions of size and IKE, while instantaneous local SST near the TC core is more important for the forecast of maximum wind speed.

1. Introduction

Tropical cyclones (TCs) are a major threat to human lives and properties in coastal areas, and predicting their characteristics remains challenging. It has long been recognized that the sea surface temperature (SST) is of great importance to tropical cyclone formation, intensification, and maintenance (Gray, 1975; Riehl, 1954). A high-SST environment favors TC intensification mainly by increasing the surface latent heat flux feedback in the high-wind boundary layer under the eyewall (Emanuel, 1986, 1995), the subsequent diabatic heating in the eyewall at midlevel (Simpson & Riehl, 1958), and the compressional warming in the eye of mature TCs due to the subsidence from its secondary circulation (Hawkins & Rubsam, 1968; Houze, 2010; Frank, 1977; Stern & Nolan, 2012).

The SST influences TC intensification on different temporal scales (Bender & Ginis, 2000; Emanuel et al., 2004; Schade & Emanuel, 1999). The average TC intensity has been shown to increase by 3–4%/C for the late 21st century (Knutson et al., 2010, 2015) and in idealized model experiments (Wang & Toumi, 2018a). The change is mainly attributed to the enhancement of latent heat flux at sea surface, rather than the change in the atmospheric lapse rate (Wang & Toumi, 2018a). On the other hand, local thermal features in the ocean, such as mesoscale oceanic temperature anomalies, can also generate considerable impact on TC intensity. For instance, Hurricanes Katrina and Rita deepened to Category 5 TCs when propagating over the bulge of the warm Loop Current, and then both weakened to Category 3 status after passing over cold-core eddies (Jaimes & Shay, 2009). TC intensity responds more dramatically to the short-term SST anomalies than the perturbation under anthropogenic warming. This is mainly because of a lack of time to reach the atmospheric radiative-convective equilibrium for the short-term or small-scale SST perturbations.

The TC outer size (radius of gale force winds), another important factor of TC destructiveness, also responds to SST changes but in a more complex way. Emanuel (1986) showed that, from a theoretical point of view, the TC horizontal extent can be scaled by the ratio of the potential intensity to the Coriolis parameter. Kharin-dinov and Emanuel (2013) and Chavas and Emanuel (2014) found a systematically positive response of TC size to a large range of SST rising (from 21 to 36 °C and from 12 to 37 °C, respectively). However, when the SST rising is reduced to 24–32 °C, Held and Zhao (2008) could only speculate the positive dependence of TC size on SST, based on a decline of the total simulated TC number in a given modeling domain with increasing SST. The change in TC size was even harder to detect when the SST was only modified from 26 to 30 °C under equilibrium conditions (Wang & Toumi, 2018a), which is a closer range to the tropical SST variation

in the current climate. This weak dependence coincides with an observational study by Knaff et al. (2014), who found no significant long-term trends of the TC size for the period 1995–2011.

As described above, both intensity and size are strongly related to SST changes. The interaction between mesoscale oceanic temperature anomalies and TCs are common in nature. Over 90% of the TCs in the western Pacific, for example, encountered at least one eddy in their lifetime (Ma et al., 2017). The impact of mesoscale temperature anomalies on TC intensity has already been extensively studied (Chan et al., 2001; Jaimes et al., 2016; Jaimes & Shay, 2009; Lin et al., 2005, 2008; Ma et al., 2017; Shay et al., 2000; Wu et al., 2007; Walker et al., 2014; Yablonsky & Ginis, 2013). There is an agreement that intensification occurs when a TC core encounters a warm anomaly due to the enhanced latent heat flux at the sea surface (and vice versa for a cold anomaly). However, the impact of mesoscale temperature anomalies on TC size has received very little attention.

The objective of this study is to investigate the response of both TC intensification and, crucially, size change to mesoscale oceanic temperature anomalies with a series of idealized simulations. Based on the aforementioned studies on the impact of SST on TC structure change, and considering the frictional dissipation dependence on the TC radial wind speed variation, we hypothesize that

1. a size increase (decrease) occurs at the same time as the intensification (deintensification) when a TC passes over a warm (cold) anomaly;
2. the increase (decrease) of TC size is mainly attributed to the change of diabatic heating in the rainbands, and thus has a strong relationship with the storm total rainfall; and
3. this size effect is retained following the mesoscale SST variation outlasting the immediate impact of the warm or cold anomaly patch on intensity.

The Advanced Weather Research and Forecasting model version 3.9 (Skamarock et al., 2008) (hereafter WRF) is used to simulate idealized tropical cyclones on an aqua planet with an f plane assumption (20°N). Three nested domains are used with horizontal grid spacing and time steps of 27 km and 90 s, 9 km and 30 s, and 3 km and 15 s, respectively. All model domains are configured with 41 sigma vertical levels and a meshgrid of 600 by 600 points. The outermost domain is large enough to prevent the anticyclonic outflow from interfering with the boundaries when the cyclone is mature and expands in size.

The model is parameterized with the Mellor-Yamada-Janjić planetary boundary layer scheme (Janjić, 1994), the Eta similarity surface layer scheme (Janjić, 2002), the WRF single-moment six-class microphysics scheme (Hong & Lim, 2006), and the rapid radiative transfer model for general circulation models (Iacono et al., 2008) for long- and short-wave radiations. The diurnal cycle of short-wave radiation is removed by fixing the solar zenith angle at 51.7° and reducing the solar constant to 685 W m^{-2} (Tompkins & Craig, 1998). The cumulus scheme is not activated in any domain since most TC-related convection can be resolved by the innermost domain; this is in agreement with Chan and Chan (2015). Finally, all domains are two-way interactive.

In the control experiment (CTRL), the SST is maintained at 27°C during the whole simulation. For the same SST, an atmospheric-sounding profile adjusted to the radiative-convective equilibrium is taken from Wang and Toumi (2018a) to prescribe the initial environmental condition and the lateral boundary condition that is fixed during the simulation. The initial state consists of a weak depression with 10 m/s near-surface winds at a radius of 80 km and generated from an analytic wind profile formulation (Wang et al., 2015). The CTRL run lasts for 13 simulated days and is not coupled with an ocean model to account for air-sea interactions.

Sensitivity experiments are performed by restarting the CTRL at the beginning of the third simulated day as well as after the seventh day when the cyclone size growth slows down. In these sensitivity simulations, a constant temperature anomaly is gradually added onto the background SST from the west boundary; however, the SST anomaly is set to $\pm 2^{\circ}\text{C}$. After a day of simulation, the full temperature anomaly is present in the domain, west of the cyclone center (see green bands in Figure 1 and supporting information Figure S1). The location of the temperature anomaly is updated at every time step so that we can emulate a cyclone approaching, crossing, and leaving an ocean SST anomaly. When the temperature anomaly center is located 600 km away on the east of the TC center, the anomaly is gradually removed from the background SST,

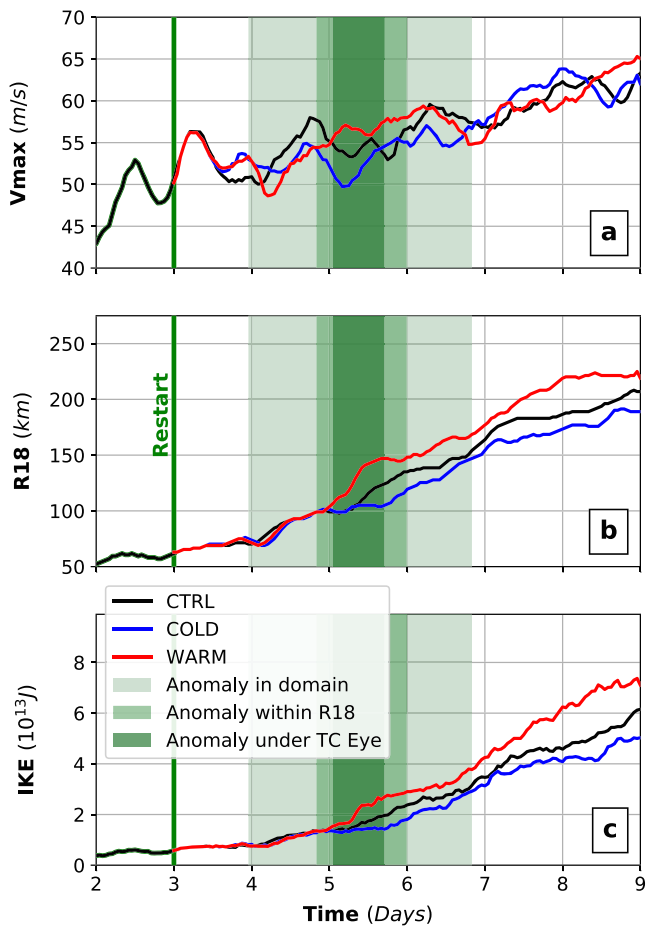


Figure 1. Response of cyclone characteristics to the presence of a warm or cold SST anomaly. (a) Maximum wind speed (V_{\max}), (b) radius of Gale force wind (18 m/s, R_{18}), and (c) integrated kinetic energy (IKE). The green vertical line illustrates the 3-day spin-up while the dark, red, and blue lines represent the CTRL, WARM, and COLD SST anomalies, respectively. Periods where the SST anomaly that enters the domain, is within R_{18} and under the cyclone eye are given by the different green-shaded regions.

the range of V_{\max} variability similar to previous studies (Chan et al., 2001; Ma et al., 2017). Similar behavior is seen with a 7-day restart when the cyclone is in a more mature stage (Figure S1a in the supporting information).

The behavior of the cyclone size is very different from intensity. Figure 1b shows large and consistent differences in gale force wind radii between the experiments. Particularly, the cyclone size expands (decreases) for the WARM (COLD) experiments, and crucially, the size does not return to the control after the TC passes the SST anomaly region (unlike the maximum wind speed). By Day 8 (over 2 days after the cyclone center exits the temperature anomaly), R_{18} is still around 10–20% larger in WARM run and 5–15% smaller in COLD run. The destructive potential of a cyclone is due to not only its intensity but also a strong function of its size. The IKE shows similar behavior to size with changes reaching +30% (−20%) for the WARM (COLD) experiment. Again, the behavior also applies to a more mature cyclone (tested through different restart times - Figures S1b and S1c in the supporting information).

The different size evolution can be understood in terms of the changes in the horizontal diabatic heating profile. The averaged azimuthal profiles for the wind speed, the radial inflow, the 400-hPa diabatic heating, and the absolute angular momentum flux (AAMF) (Chan & Chan, 2013) are shown in Figure 2. We consider three 1-day average stages: before the SST anomaly enters R_{18} (Figures 2a, 2d, and 2g), when the cyclone center is over the anomaly (Figures 2b, 2e, and 2h) and when the SST anomaly has exited R_{18} (Figures 2c, 2f, and 2i).

which is a similar but reversed process as adding the temperature anomaly in (supporting information Figure S2 shows the time evolution of the radial profile of surface heat fluxes, highlighting the presence of no discontinuity induced by the appearance of the SST anomaly).

The SST anomalies are characterized by three parameters: geometric radius, temperature strength, and moving speed relative to TC center. In the warm and cold experiments (hereafter WARM and COLD), the parameters are set to 150-km radius (i.e., an idealized square anomaly of 300 km by 300 km), an SST anomaly of $\pm 2^{\circ}\text{C}$ and a moving speed of 5 m/s. Based on the WARM and COLD experiments, more sensitivity experiments are conducted by perturbing one of the three parameters independently while the others are fixed to the reference case (150-km radius, 5-m/s moving speed, and $\pm 2^{\circ}\text{C}$ anomaly), that is,

- 75, 150, and 225 km radius;
- $\pm 1, \pm 2$, and $\pm 3^{\circ}\text{C}$ temperature anomaly; and
- 3, 5, and 7 m/s moving speed.

The geometric size and relative moving speed in the WARM and COLD experiments agree with the typical values of ocean mesoscale eddies (Kossin, 2018; Ma et al., 2017). One CTRL run and 14 sensitivity runs have been carried out for 3-day and 7-day restart time, respectively (29 runs in total). The three key experiments (CTRL, WARM, and COLD) will first be used to investigate the physical mechanisms that will then be confirmed with the sensitivity experiments.

3. Results

Figure 1 shows the response of maximum wind speed (V_{\max}), gale force wind radius (18 m/s, R_{18}), and integrated kinetic energy (Powell & Reinhold, 2007; Wang & Toumi, 2016) (IKE) to the presence of a $\pm 2^{\circ}\text{C}$ SST anomaly patch. The intensity response is quite weak (around 5%) and almost instantaneous (a few hours lag) to the SST change with (de)-intensification of V_{\max} for the WARM (COLD) experiments compared to the CTRL run (Figure 1a). However, when the TC center exits and travels away from the anomaly, the TC intensity returns to similar levels of the control experiment after around 12 hr. These changes are in

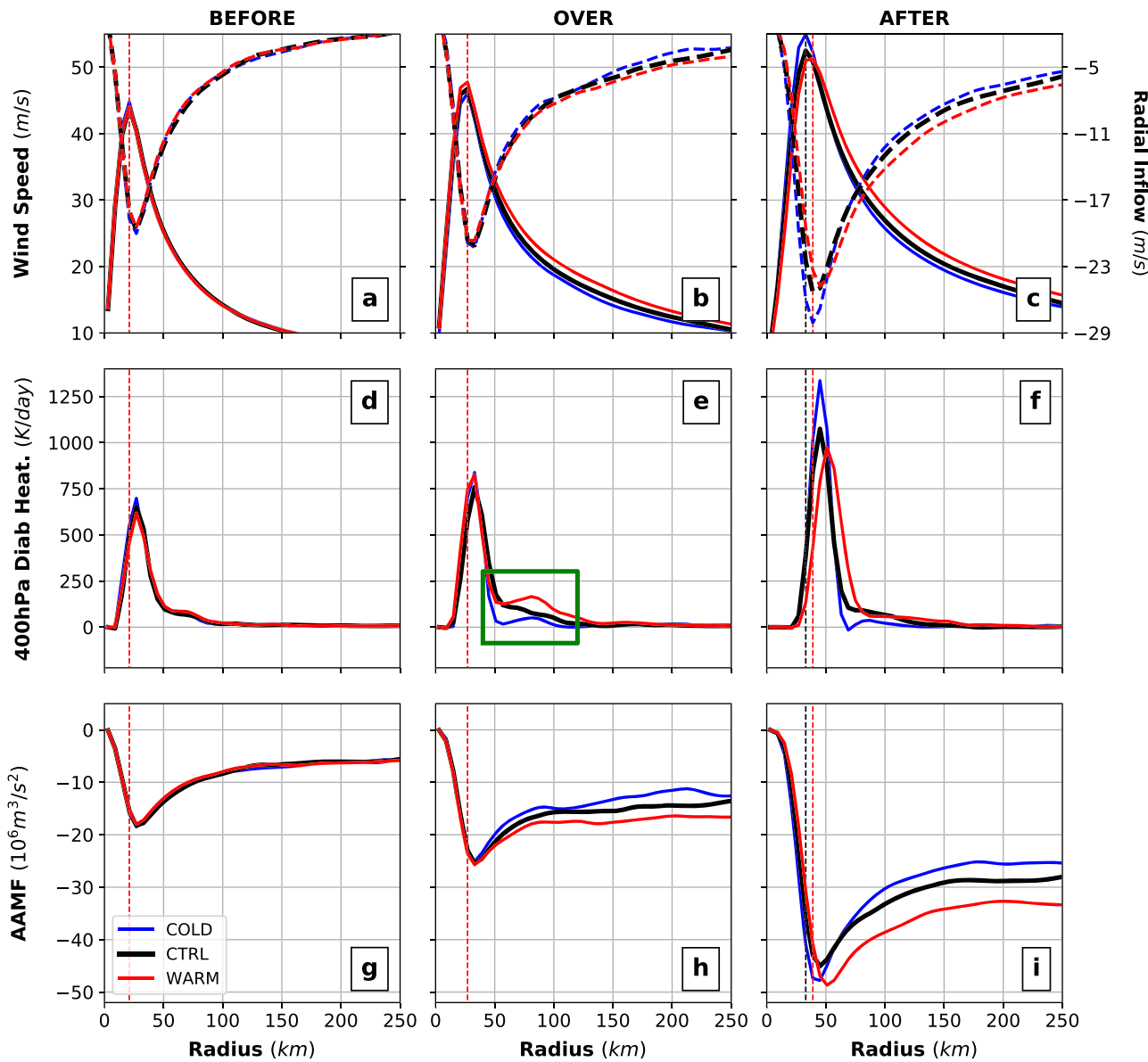


Figure 2. One-day-averaged azimuthal-mean radial profiles of key cyclone properties: (a–c) 10-m wind profiles superimposed on radial inflow (dashed lines) and R_{\max} (vertical dotted lines) before, over or after the SST anomaly, respectively; (d–f) 400 hPa diabatic heating profiles; (g–i) 10 m absolute angular momentum flux (AAMF) profiles. The time average period is set to 1 day; the OVER diagnostics are defined when the cyclone eye is over the SST anomaly (between day 4.9 and 5.9, center panels). The BEFORE diagnostics are averaged before the anomaly is within R_{18} (from around 3.3 to 4.3 days, left panels), while the AFTER diagnostics are computed after the SST anomaly exits R_{18} (from around 7 to 8 days, right panels). Dark, red, and blue lines represent the CTRL, WARM, and COLD SST anomalies, respectively. Green box in Figure 2e highlights the change of diabatic heating between the experiments.

- Before meeting the anomaly, the cyclone develops over a constant SST and is not exposed to the SST anomaly. All three experiments lead to similar azimuthal wind profiles (small differences mainly due to the initial impact of the SST anomaly and the ambient thermodynamic adjustment), with V_{\max} of about 45 m/s and R_{\max} of 20 km. Due to the outward tilting of the eyewall, the peak of the 400-hPa diabatic heating is at a larger radius than the peak of 10-m wind speed.
- When the cyclone is over the anomaly, the 1-day average intensity and R_{\max} remain similar (25 km) in the three simulations. However, while the peak near the eyewall of 400-hPa diabatic heating is comparable between the experiments, a clear increase/decrease of the diabatic heating in the rainbands (60–125 km) is visible between the different experiments (green box in Figure 2e and surface heat fluxes in Figure S2). This is associated with a local AAMF (de)increase (Holland & Merrill, 1984; Willoughby et al., 1982).

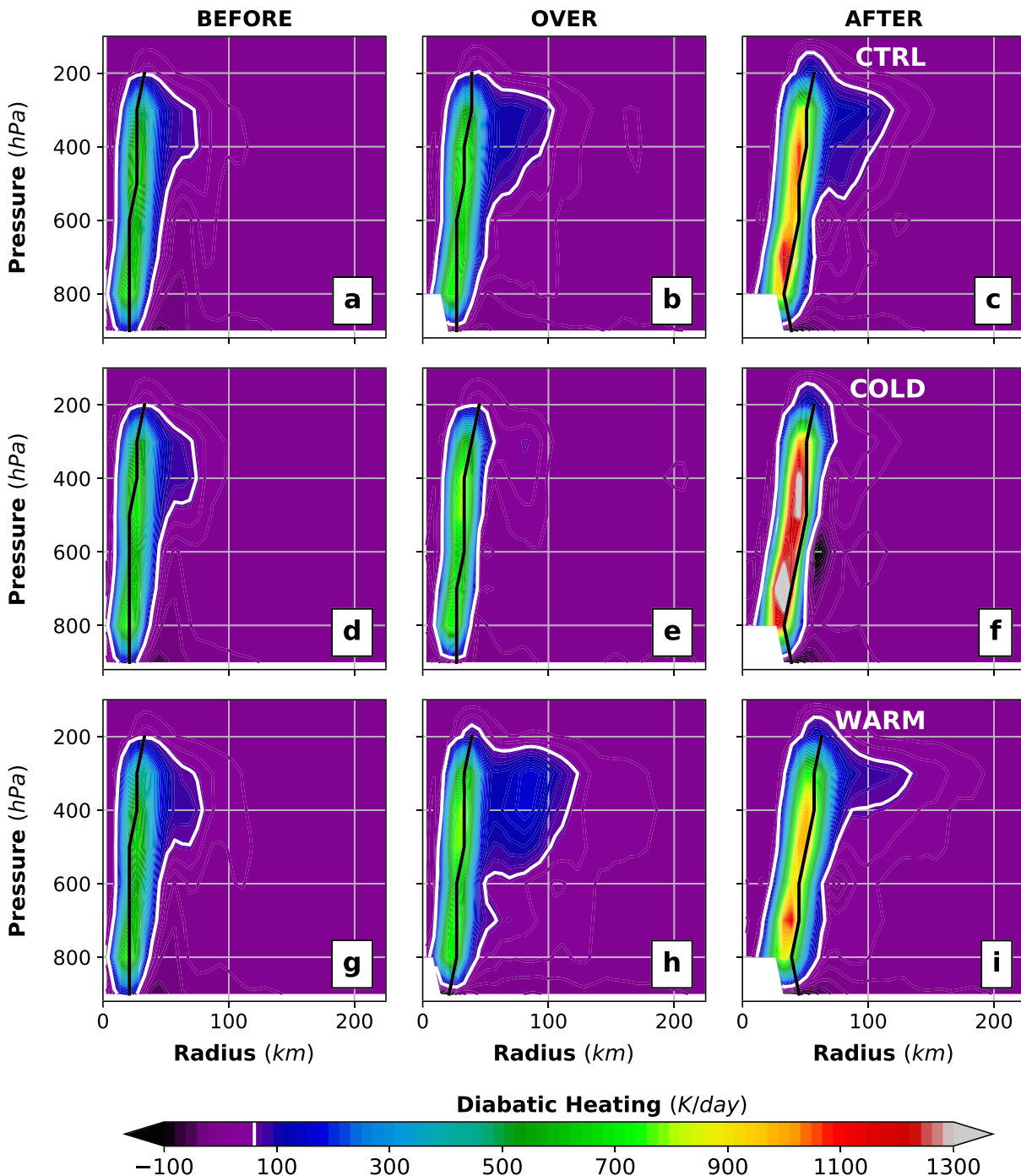


Figure 3. One-day-averaged azimuthal-mean vertical profiles of 400-hPa diabatic heating. Top panels (a–c) show the CTRL experiment, middle panels (d–f) the COLD experiment, and the bottom panels (g–i) the WARM experiment. See Figure 2 for the averaging period definition. The plain dark lines show the radius of maximum wind at each level, while the plain white lines show the 60-K/day diabatic heating contour.

Therefore, (less) more momentum is radially transported into the system in the rainband region and the cyclone size (de)increases for the (COLD) WARM simulations.

- After crossing the SST anomaly, the WARM experiment shows a larger R_{\max} and R_{18} and a wider AAMF remaining at all radii, reenforcing the transport of momentum into the cyclone, while wind speeds and radial inflows have larger tails (the opposite occurs for the COLD simulation). The COLD run, though, shows slightly higher V_{\max} , radial inflows and diabatic heating as the cyclone is starting its expansion later than the CTRL and WARM cases creating a time lag in the cyclone development phase.

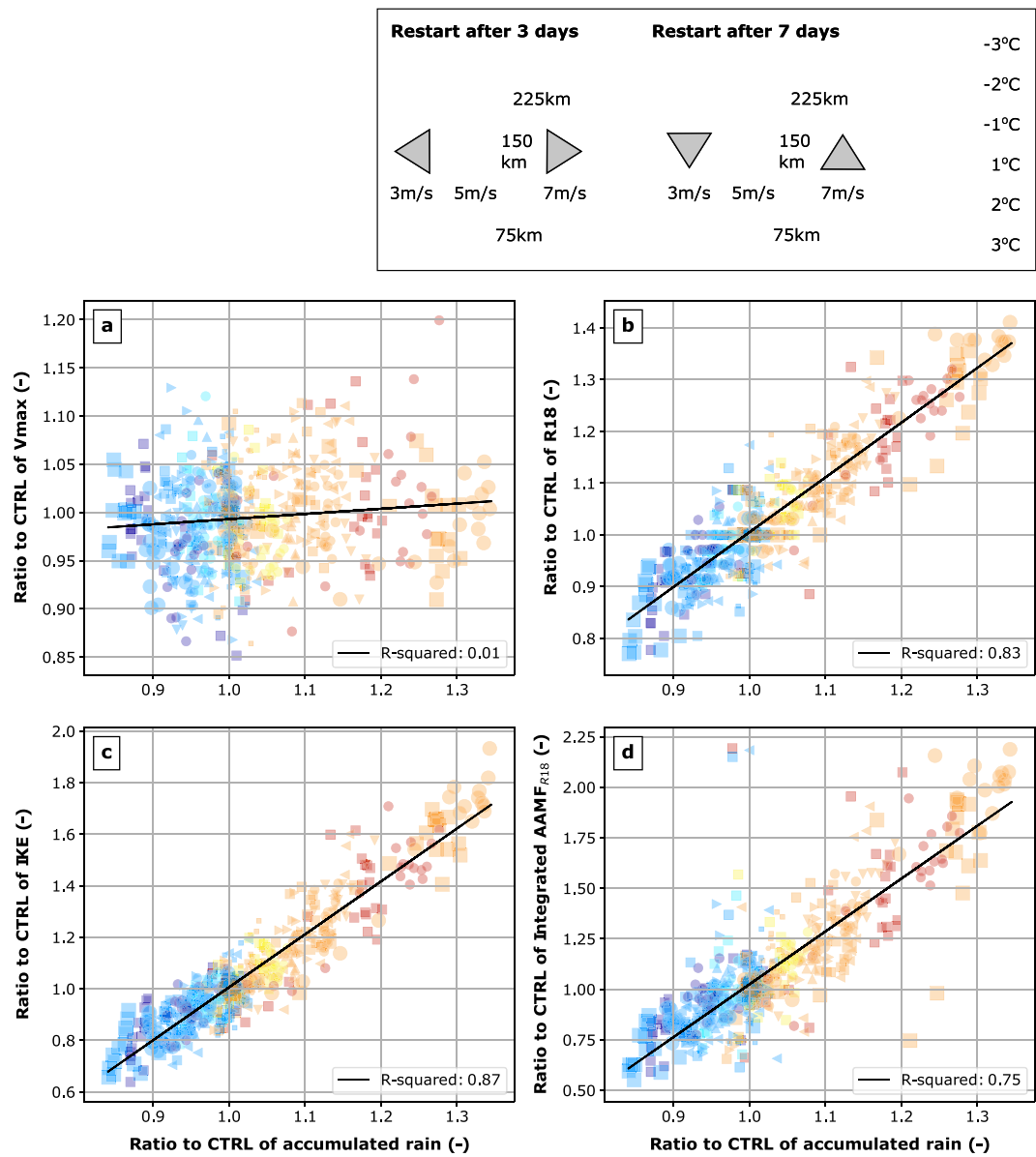


Figure 4. Ratio to CTRL simulation of maximum wind speed V_{max} (a), Gale force wind radius R_{18} (b), integrated kinetic energy IKE (c), and integrated absolute angular momentum flux at R_{18} (d) as a function of the ratio (to CTRL) of past integrated accumulated rain within 600 km of the cyclone eye (integrated since the restart time). Each marker represents 6-hourly time stamps.

Figure 3 shows the averaged vertical azimuthal profile of diabatic heating for the same three phases (before, over, and after the anomaly) and supporting information Figure S3 illustrates the time evolution of the 400-hPa diabatic heating. For the WARM case, over the anomaly (Figures 3b, 3e, and 3h), the development of the diabatic heating in the rainbands is clearly seen and is due to enhanced surface heat flux and more enthalpy going into the system. The heat is transported into the core and released in the eyewall at midlevel. The COLD experiment leads to the opposite behaviors. After the anomaly crossing, the peak diabatic heating is stronger for the COLD experiment and weaker for the WARM. The extension in the rainbands region starts for the COLD experiment, while the CTRL shows larger diabatic heating than in the WARM experiment (both in magnitude and extension in the rainbands). This tends to highlight a temporal lag in the development of the cyclone between the different experiments with the COLD case developing with few hours delay compared to the WARM case (Figure 1).

Sensitivity analyses have been carried out for a range of SST anomaly sizes from 75 to 225 km, transitional speeds from 3 to 7 m/s, and intensities of the temperature anomaly from ± 1 to 3°C as well as cyclone maturity. The simulations presented in this study were set to use average realistic characteristics. As anticipated, larger and more intense anomalies or slower moving cyclones lead to larger differences. Figure 4 summarizes sensitivity experiences as a ratio to the CTRL simulation of a range of variables (V_{\max} , R_{18} , *IKE*, and integrated AAMF at R_{18}) function of the ratio (to CTRL) of storm total precipitation (as a proxy of diabatic heating) within 600 km of the cyclone eye and accumulated in time (supporting information Figure S4 shows the same but as a function of the ratio (to CTRL) of integrated sensible and latent heat fluxes). While the maximum wind speed shows no apparent link to the storm total precipitation or integrated heat flux, R_{18} and *IKE* clearly highlight strong correlations ($R^2 > 0.8$). Note that the *IKE* variability is also partially driven by V_{\max} . The R_{18} is directly proportional to the integrated heat input. The integrated AAMF at R_{18} also shows correlations to the precipitation and heat ($R^2 > 0.7$). In addition, similar analyses are carried out for the inner (0–100 km from the eye) and the outer (100–600 km from the eye) cyclone regions. While no correlation is found for each of the four cyclone characteristics within 100 km of the cyclone center, the outer region exhibits correlation of around 0.5, highlighting the importance of the rainband regions (results no shown). This corroborates the dynamics detailed above.

4. Discussion and Summary

In the WARM experiment (the behavior for the COLD is similar but reversed), when the cyclone is over the anomaly, the surface heat flux is enhanced. The extra enthalpy is fluxed into the TC boundary layer, resulting in an extra moisture convergence at the TC core. Due to the eyewall ascending and subsequent condensation, the additional latent heat is released at midlevels and the strong diabatic heating in the eyewall drives the rapid intensification. After crossing the warm SST anomaly, the thermodynamic disequilibrium between the TC boundary layer and the sea surface adjusts relatively rapidly toward the control state, which leads to return to preanomaly surface enthalpy flux and subdued ascending flow in the eyewall. A relatively weak secondary circulation can no longer sustain the high near-surface winds against the surface dissipation. Consequently, the cyclone restores back toward the control experiment condition. Our simulations show a recovery of the cyclone intensity to the control value with a turnover time of about 12–24 hr. The momentum of the core is approximately in steady-state with horizontal advection balanced by vertical advection and frictional loss. The impact of SST anomalies on intensity is therefore a shorter term, and there is no long-term memory of SST history in the cyclone intensity.

The picture is very different for the size change. When over the warm SST anomaly, the enhancement of diabatic heating in the eyewall accelerates the secondary circulation, leading to an increase of inflow in the boundary layer. Therefore, the angular momentum flux increases, transporting extra momentum into the cyclone core, which ultimately drives the size growth (Chan & Chan, 2013). The Earth angular momentum at large radii acts as a momentum reservoir to support the TC size increase. A key feature related to the size growth is the emerging structure of diabatic heating outside the eyewall (green box in Figure 2e). Even after crossing the warm SST anomaly, due to the extra heating in the rainbands, the TC size remains larger than the control run. This linkage between the rainbands heating and TC outer size has been previously shown (Hill & Lackmann, 2009; Wang, 2009). Unlike for the core momentum, the outer momentum is not in steady state as the horizontal momentum import exceeds the sum of the local loss and the further inward advection, and thus the circulation expands.

The different time scale of adjusting to momentum perturbations, for example, at the core and the outer region is a reason for the long memory of the TC outer size. The time scale of surface adjustment can be estimated from the ratio of the wind speed to the surface drag. The surface turbulent drag is proportional to the square of the wind speed. The ratio of the time scales is therefore approximately given by the ratio of the wind speeds (assuming similar drag coefficients). In the case of comparing the time scale at R_{\max} and R_{18} that would lead to about a factor of 3 ($V_{\max}/V_{18} = 55 \text{ m s}^{-1}/18 \text{ m s}^{-1}$, Figure 1a). This suggests that it would take about 3 times longer to dissipate the outer surface winds against friction than at the core. A steady state is only rapidly achieved under the eyewall.

By the end of the simulations, the outer size does not appear to reach an equilibrium state which could lead to uncertainties. Chavas and Emanuel (2014) identified an equilibrium after more than two simulation months in an idealized axisymmetric modeling framework. This study focuses on the evolution of TC wind

structure within a realistic time scale relative to a TC life span (10 days). The temporal evolution of cyclone characteristics (intensity and size) is in agreement with previous 3-D model studies (Chan et al., 2001; Ma et al., 2017). Furthermore, a recent observational study (Wang & Toumi, 2018b) showed that the composited prelandfall TC outer size continues expanding before losing energy inputs, which is consistent with the simulated size evolution in this study. Moreover, the different dissipation time scales, as explained previously, are independent of the general evolution of TC wind field. This suggests that even if a TC encounters a temperature anomaly after reaching an equilibrium outer size (if possible in the real world), the long memory effect as found in this study should hold.

The TC size at any time can be significantly impacted by a region with a different SST (see Figure 4), and these SST-induced size changes are not quickly restored when the cyclone has crossed the anomaly. The size and integrated kinetic energy can be considered as path dependent as they are a consequence of the integrated ocean surface heat flux along the whole track. This path dependence creates a long memory in the size. By analogy the intensity may be considered state dependent with short memory. These different time scales of adjustment may also explain why observations only show a weak relationship between size and intensity (Merrill, 1984; Weatherford & William, 1988). The forecast of the TC size and the integrated kinetic energy may have a larger uncertainty than intensity as the forecast error of size would be a combination of TC wind and SST uncertainties accumulated along the track, whereas the instantaneous intensity error is more influenced by the local SST uncertainty.

Acknowledgments

The present study was supported by the UK-China Research and Innovation Partnership Fund through the Met Office Climate Science for Service Partnership (CSSP) China as part of the Newton Fund. S. W. is also supported by the National Natural Science Foundation of China (Grant 41706007). Simulations were carried out on the Imperial College High Performance Computing Service (doi: 10.14469/hpc/2232). Model outputs used in this study are available at the Imperial College High Performance Computing Service Data Repository (<https://doi.org/10.14469/hpc/6696>). The full model outputs will be made available upon request to the authors.

References

- Bender, M. A., & Ginis, I. (2000). Real-case simulations of hurricane-ocean interaction using a high-resolution coupled model: Effects on hurricane intensity. *Monthly Weather Review*, 128(4), 917–946. [https://doi.org/10.1175/1520-0493\(2000\)128<0917:RCOSHO>2.0.CO;2](https://doi.org/10.1175/1520-0493(2000)128<0917:RCOSHO>2.0.CO;2)
- Chan, K. T., & Chan, J. C. (2013). Angular momentum transports and synoptic flow patterns associated with tropical cyclone size change. *Monthly Weather Review*, 141(11), 3985–4007.
- Chan, K. T. F., & Chan, J. C. L. (2015). Impacts of vortex intensity and outer winds on tropical cyclone size. *Quarterly Journal of the Royal Meteorological Society*, 141(687), 525–537. <https://doi.org/10.1002/qj.2374>
- Chan, J. C. L., Duan, Y., & Shay, L. K. (2001). Tropical cyclone intensity change from a simple ocean-atmosphere coupled model. *Journal of the Atmospheric Sciences*, 58(2), 154–172. [https://doi.org/10.1175/1520-0469\(2001\)058<0154:TCICFA>2.0.CO;2](https://doi.org/10.1175/1520-0469(2001)058<0154:TCICFA>2.0.CO;2)
- Chavas, D. R., & Emanuel, K. (2014). Equilibrium tropical cyclone size in an idealized state of axisymmetric radiative-convective equilibrium. *Journal of the Atmospheric Sciences*, 71(5), 1663–1680.
- Emanuel, K. A. (1986). An air-sea interaction theory for tropical cyclones. Part I: Steady-state maintenance. *Journal of the Atmospheric Sciences*, 43(6), 585–605.
- Emanuel, K. A. (1995). Sensitivity of tropical cyclones to surface exchange coefficients and a revised steady-state model incorporating eye dynamics. *Journal of the Atmospheric Sciences*, 52(22), 3969–3976.
- Emanuel, K., DesAutels, C., Holloway, C., & Korty, R. (2004). Environmental control of tropical cyclone intensity. *Journal of the Atmospheric Sciences*, 61(7), 843–858. [https://doi.org/10.1175/1520-0469\(2004\)061<0843:ECOTCI>2.0.CO;2](https://doi.org/10.1175/1520-0469(2004)061<0843:ECOTCI>2.0.CO;2)
- Frank, W. (1977). The structure and energetics of the tropical cyclone. Part I: Storm structure. *Monthly Weather Review*, 105, 1119–1135.
- Gray, W. M. (1975). Tropical cyclone genesis. Colorado State University.
- Hawkins, H., & Rubsam, D. (1968). Hurricane Hilda, 1964. *Monthly Weather Review*, 96, 617–636.
- Held, I. M., & Zhao, M. (2008). Horizontally homogeneous rotating radiative-convective equilibria at GCM resolution. *Journal of the Atmospheric Sciences*, 65(6), 2003–2013.
- Hill, K. A., & Lackmann, G. M. (2009). Influence of environmental humidity on tropical cyclone size. *Monthly Weather Review*, 137(10), 3294–3315. <https://doi.org/10.1175/2009MWR2679.1>
- Holland, G. J., & Merrill, R. T. (1984). On the dynamics of tropical cyclone structural changes. *Quarterly Journal of the Royal Meteorological Society*, 110(465), 723–745. <https://doi.org/10.1002/qj.49711046510>
- Hong, S.-Y., & Lim, J.-O. J. (2006). The WRF single-moment 6-class microphysics scheme (WSM6). *Journal of the Korean Meteorological Society*, 42(2), 139–151.
- Houze, R. A. (2010). Clouds in tropical cyclones. *Monthly Weather Review*, 138(2), 293–344. <https://doi.org/10.1175/2009MWR2989.1>
- Iacono, M. J., Delamere, J. S., Mlawer, E. J., Shephard, M. W., Clough, S. A., & Collins, W. D. (2008). Radiative forcing by long-lived greenhouse gases: Calculations with the AER radiative transfer models. *Journal of Geophysical Research*, 113, D13103. <https://doi.org/10.1029/2008JD009944>
- Jaimes, B., & Shay, L. K. (2009). Mixed layer cooling in mesoscale oceanic eddies during Hurricanes Katrina and Rita. *Monthly Weather Review*, 137(12), 4188–4207. <https://doi.org/10.1175/2009MWR2849.1>
- Jaimes, B., Shay, L. K., & Brewster, J. K. (2016). Observed air-sea interactions in tropical cyclone isaac over loop current mesoscale eddy features. *Dynamics of Atmospheres and Oceans*, 76, 306–324.
- Janjic, Z. I. (1994). The step-mountain eta coordinate model: Further developments of the convection, viscous sublayer, and turbulence closure schemes. *Monthly Weather Review*, 122, 927–945.
- Janjic, Z. I. (2002). Nonsingular implementation of the Mellor-Yamada level 2.5 scheme in the NCEP MESO model. NCEP Office Note 61.
- Khairoutdinov, M., & Emanuel, K. (2013). Rotating radiative-convective equilibrium simulated by a cloud-resolving model. *Journal of Advances in Modeling Earth Systems*, 5, 816–825. <https://doi.org/10.1002/2013MS000253>
- Knaff, J. A., Longmore, S. P., & Molenar, D. A. (2014). An objective satellite-based tropical cyclone size climatology. *Journal Climate*, 27(1), 455–476.
- Knutson, T. R., McBride, J. L., Chan, J., Emanuel, K., Holland, G., Landsea, C., et al. (2010). Tropical cyclones and climate change. *Nature Geoscience*, 3, 157–163.

- Knutson, T. R., Sirutis, J. J., Zhao, M., Tuleya, R. E., Bender, M., Vecchi, G. A., et al. (2015). Global projections of intense tropical cyclone activity for the late twenty-first century from dynamical downscaling of CMIP5/RCP4.5 Scenarios. *Journal Climate*, 28(18), 7203–7224.
- Kossin, J. (2018). A global slowdown of tropical-cyclone translation speed. *Nature*, 558(7708), 104–107.
- Lin, I., Wu, C.-C., Emanuel, K. A., Lee, I.-H., Wu, C.-R., & Pun, I.-F. (2005). The interaction of supertyphoon Maemi (2003) with a warm ocean eddy. *Monthly Weather Review*, 133(9), 2635–2649.
- Lin, I.-I., Wu, C.-C., Pun, I.-F., & Ko, D.-S. (2008). Upper-ocean thermal structure and the western North Pacific category 5 typhoons. Part I: Ocean features and the category 5 typhoons intensification. *Monthly Weather Review*, 136(9), 3288–3306. <https://doi.org/10.1175/2008MWR2277.1>
- Ma, Z., Fei, J., Liu, L., Huang, X., & Li, Y. (2017). An investigation of the influences of mesoscale ocean eddies on tropical cyclone intensities. *Monthly Weather Review*, 145(4), 1181–1201. <https://doi.org/10.1175/MWR-D-16-0253.1>
- Merrill, R. T. (1984). A comparison of large and small tropical cyclones. *Monthly Weather Review*, 112(7), 1408–1418.
- Powell, M. D., & Reinhold, T. A. (2007). Tropical cyclone destructive potential by integrated kinetic energy. *Bulletin of the American Meteorological Society*, 88(4), 513–526. <https://doi.org/10.1175/BAMS-88-4-513>
- Riehl, H. (1954). Tropical meteorology. McGraw-Hill.
- Schade, L. R., & Emanuel, K. A. (1999). The ocean's effect on the intensity of tropical cyclones: Results from a simple coupled atmosphere-ocean model. *Journal of the Atmospheric Sciences*, 56(4), 642–651. [https://doi.org/10.1175/1520-0469\(1999\)056<0642:TOSEOT>2.0.CO;2](https://doi.org/10.1175/1520-0469(1999)056<0642:TOSEOT>2.0.CO;2)
- Shay, L. K., Goni, G. J., & Black, P. G. (2000). Effects of a warm oceanic feature on hurricane opal. *Monthly Weather Review*, 128(5), 1366–1383.
- Simpson, R., & Riehl, R. (1958). Mid-tropospheric ventilation as a constraint on hurricane development and maintenance. Preprints, Tech. Conf. on hurricanes, Miami Beach, Fl, Amer. Meteor. Soc. Tech. rep., D4-1-D4-10.
- Skamarock, W. C., Klemp, J. B., Dudhia, J., Gill, D. O., Barker, D. M., Duda, M., et al. (2008). A description of the advanced research WRF version 3. NCAR Technical Note.
- Stern, D. P., & Nolan, D. S. (2012). On the height of the warm core in tropical cyclones. *Journal of the Atmospheric Sciences*, 69(5), 1657–1680. <https://doi.org/10.1175/JAS-D-11-010.1>
- Tompkins, A. M., & Craig, G. C. (1998). Radiative-convective equilibrium in a three-dimensional cloud-ensemble model. *Quarterly Journal of the Royal Meteorological Society*, 124(550), 2073–2097.
- Walker, N. D., Leben, R. R., Pilley, C. T., Shannon, M., Herndon, D. C., Pun, I.-F., et al. (2014). Slow translation speed causes rapid collapse of Northeast Pacific Hurricane Kenneth over cold core eddy. *Geophysical Research Letters*, 41, 7595–7601. <https://doi.org/10.1002/2014GL061584>
- Wang, Y. (2009). How do outer spiral rainbands affect tropical cyclone structure and intensity? *Journal of the Atmospheric Sciences*, 66(5), 1250–1273.
- Wang, S., & Toumi, R. (2016). On the relationship between hurricane cost and the integrated wind profile. *Environmental Research Letters*, 11, 114,005. <https://doi.org/10.1088/1748-9326/11/11/114005>
- Wang, S., & Toumi, R. (2018a). Reduced sensitivity of tropical cyclone intensity and size to sea surface temperature in a radiative-convective equilibrium environment. *Advances in Atmospheric Sciences*, 35, 981–993. <https://doi.org/10.1007/s00376-018-7277-5>
- Wang, S., & Toumi, R. (2018b). A historical analysis of the mature stage of tropical cyclones. *International Journal of Climatology*, 38, 2490–2505. <https://doi.org/10.1002/joc.5374>
- Wang, S., Toumi, R., Czaja, A., & Van Kan, A. (2015). An analytic model of tropical cyclone wind profiles. *Quarterly Journal of the Royal Meteorological Society*, 141, 3018–3029. <https://doi.org/10.1002/qj.2586>
- Weatherford, C. L., & William, M. G. (1988). Typhoon structure as revealed by aircraft reconnaissance. Part I: Data analysis and climatology. *Monthly Weather Review*, 116(5), 1032–1043.
- Willoughby, H. E., Clos, J. A., & Shoreibah, M. G. (1982). Concentric eye walls, secondary wind maxima, and the evolution of the hurricane vortex. *Journal of the Atmospheric Sciences*, 39(2), 395–411. [https://doi.org/10.1175/1520-0469\(1982\)039<0395:CEWSWM>2.0.CO;2](https://doi.org/10.1175/1520-0469(1982)039<0395:CEWSWM>2.0.CO;2)
- Wu, C.-C., Lee, C.-Y., & Lin, I. (2007). The effect of the ocean eddy on tropical cyclone intensity. *Journal of the Atmospheric Sciences*, 64(10), 3562–3578.
- Yablonsky, R. M., & Ginis, I. (2013). Impact of a warm ocean eddy's circulation on hurricane-induced sea surface cooling with implications for hurricane intensity. *Monthly Weather Review*, 141(3), 997–1021.

Erratum

In the originally published version of this article, the title was published incorrectly. This error has since been corrected, and the present version may be considered the authoritative version of record.